Multi-stage Coordinated Robust Optimization for Soft Open Point Allocation in Active Distribution Networks with PV

Anqi Tao, Niancheng Zhou, Yuan Chi, Qianggang Wang, and Guangde Dong

***Abstract*—To optimize the placement of soft open points (SOPs) in active distribution networks (ADNs), many aspects should be considered, including the adjustment of transmission power, integration of distributed generations (DGs), coordination with conventional control methods, and maintenance of economic costs. To address this multi-objective planning problem, this study proposes a multi-stage coordinated robust optimization model for the SOP allocation in ADNs with photovoltaic (PV). First, two robust technical indices based on a robustness index are proposed to evaluate the operation conditions and robust optimality of the solutions. Second, the proposed coordinated allocation model aims to optimize the total cost, robust voltage offset index, robust utilization index, and voltage collapse proximity index. Third, the optimization methods of the multi- and single-objective models are coordinated to solve the proposed multi-stage problem. Finally, the proposed model is implemented on an IEEE 33-node distribution system to verify its effectiveness. Numerical results show that the proposed index can better reveal voltage offset conditions as well as the SOP utilization, and the proposed model outperforms conventional ones in terms of robustness of placement plans and total cost.**

***Index Terms*—Multi-stage coordinated optimization allocation, robustness index, soft open point (SOP), active distribution network.**

I. Introduction

RENEWABLE energy can effectively address the conflict between growing load demands and environmental protection, and these topics have received growing attention in recent years [1], [2]. However, increased integration generates problems for active distribution networks (ADNs), including bidirectional power flow, voltage rise, and power fluctuation. Soft open points (SOPs) are effective solutions to address these problems, whereby the power flow can be adjusted and a flexible connection among feeders can be realized [3]. Correspondingly, SOPs must be used both to optimize economic objectives such as reducing network loss and to meet technical requirements such as power supply reliability improvement and fluctuation suppression. SOPs are also required for coordinating with conventional control methods such as the switching of capacitor banks (CBs) and demand response (DR) to increase the integration of distributed generations (DGs) and further reduce carbon emissions. Therefore, introducing a multi-objective coordinated optimization model is critical in determining the optimal locations and capacities of SOPs in ADNs.

Numerous studies on the optimal targets of SOPs in ADNs have been conducted. References [4]-[6] optimized the total cost of a distribution network, and [7]-[10] introduced technical-oriented multi-objective optimization (that included power loss reduction, load unbalanced condition, and voltage profile improvement) to demonstrate the capabilities of SOPs in improving the operating conditions of ADNs. The objective function in [11] aimed to maximize the restoration of weighted loads based on networked microgrids formed by SOPs. However, these studies hardly considered the indices or targets related to the SOP utilization, which means that very few variables from the SOP model were used in the technical indices to measure whether the SOP utilization was reasonable. This research gap has resulted in lower active and reactive power regulation capacities and higher economic costs.

The outputs of renewable energy and load demand in ADNs are characterized by a certain degree of uncertainty. Provided that the optimization objectives are highly sensitive to the fluctuation of uncertainty factors, the effectiveness of the SOP planning is weakened. Previously, the generation of stochastic distribution functions, typical uncertainty scenarios, or robust optimization was adopted to address uncertain variables. Monte Carlo simulations were conducted in [2] and [12] to produce several scenarios to imitate the uncertainty of load demand and DGs; historical data samples were used in [3], [8], and [13] to construct uncertain scenarios to represent stochastic behavior; and Weibull and beta distributions were introduced in [14] to address uncertain factors. However, these methods are unsystematic and inaccurate for long-term allocation-related problems because it is difficult

Manuscript received: June 28, 2022; revised: August 22, 2022; accepted: August 22, 2022. Date of CrossCheck: August 22, 2022. Date of online publication: September 30, 2022.

This work was supported in part by the National Natural Science Foundation of China (General Program) (No. 52077017) and the International Postdoctoral Exchange Fellowship Program (Talent-Introduction Program) (No. YJ20210337).

A. Tao, N. Zhou, Y. Chi (corresponding author), and Q. Wang are with the State Key Laboratory of Power Transmission Equipment and System Security and New Technology, Chongqing University, Chongqing 400044, China (e-mail: mm2858112@qq.com; cee_nczhou@cqu.edu.cn; chiyuanee@cqu.edu.cn; qianggang1987@cqu.edu.cn).

G. Dong is with State Grid Chongqing Electric Power Company Limited, Chongqing 401123, China (e-mail: 1012423917@qq.com).

DOI: 10.35833/MPCE.2022.000373

to obtain the long-term fluctuation of uncertainty factors. Thus, the optimal solutions generated by these methods are not robust to uncertainty factors. Robust optimization is a desirable alternative for addressing uncertainties [15]. Two-stage robust optimization (RO) models were adopted in [10], [16], and [17] to improve robust system security. However, this type of model is based on worst-case scenarios, which leads to over-conservative results [10]. Reference [9] employed distributional RO to avoid over-conservative results. However, the solution of this model is complex and results in time-consuming computations.

For the solution method, the majority of existing multi-objective optimization methods using SOPs typically model multiple objectives as a single target with a weighted sum, such as in [10], [18], [19]. However, establishing weight parameters for practical engineering problems is subjective and oversimplified. Alternatively, multi-objective evolutionary algorithms (MOEAs) are effective at solving multi-objective optimization problems. References [20]-[23] adopted well-known MOEAs such as non-dominated sorting genetic algorithm-II (NSGA-II), particle swarm optimization, ant colony optimization, and the Archimedes optimization algorithm to obtain optimized results. Reference [24] proposed a systematic solving method for the maximum term constraint, which was combined with the ε constraint algorithm for multi-objective optimization. However, these solution methods rarely consider robustness. The number of variables, convergence difficulties, and corresponding computational burden all increase exponentially when robust optimality is considered.

To address the weaknesses of previous studies, this paper proposes a multi-stage coordinated optimization model for the SOP allocation while considering economic, robust technical, and voltage collapse proximity indices. The main contributions of this paper are summarized as follows.

1) New robust technical indices based on the quantitative robustness assessment method are proposed to evaluate the robust optimality of allocation results. These strengthen the effectiveness of the SOP allocation optimization strategy without requiring assumed probability distributions for uncertain variables.

2) A multi-stage SOP allocation optimization model is established to balance the tradeoff among the investment and operation costs, robust voltage offset index, robust SOP utilization index, and voltage collapse proximity index.

3) A coordinated multi-objective nonlinear model and single-objective linear model solution method are proposed to solve the multi-stage SOP allocation optimization model. Compared with conventional methods that consider single-objective optimization or direct multi-objective optimization, the proposed model not only avoids the subjectivity of the single-objective model but also breaks through the computational burden of direct multi-objective solvers, thereby allowing robustness to be considered.

The remainder of this paper is organized as follows. Section II presents the technical evaluation indices (robustness, robust voltage offset, robust SOP utilization, and voltage collapse proximity indices). Section III establishes the multi-stage robust optimization model. Section IV describes the computational steps, and presents a flow of the proposed solution method. Section V presents case studies, and Section VI concludes this paper.

II. Technical Evaluation Indices

A. Quantitative Robustness Assessment

The uncertainty of the output and load demand of DGs under an ADN operation can deteriorate the performance of SOPs. In this paper, a novel robustness index is proposed to assess the sensitivity of an SOP plan when subjected to uncertain variables. The acceptable sensitivity region (ASR), which represents the maximum acceptable variation of the objective function value subjected to variations in specific uncertain parameters [25], is effective for sensitivity assessment. As illustrated in [25], the result of a larger ASR is a more robust solution.

Two variations of uncertainties ($\Delta\tilde{\omega}_1$ and $\Delta\tilde{\omega}_2$ in Fig. 1) and two objectives (f_1 and f_2 in Fig. 2) are adopted to improve the robustness assessment. Figure 1 illustrates an ASR and sensitive directions when uncertainties are affiliated with the objectives. Point 1 (P1) represents a case in which the variation in f_i Δf_i is smaller than the maximum acceptable variation $\Delta f_{i\max}$. Point 2 (P2) represents a situation in which $\Delta f_i = \Delta f_{i\max}$. Point 3 (P3) represents a scenario in which $\Delta f_i > \Delta f_{i\max}$. Correspondingly, Fig. 2 shows the range of Δf_i derived from $\Delta\tilde{\omega}_i$. P1-P3 in Fig. 1 conform to P1-P3 of the Δf_i range (Fig. 2), respectively. The smaller the range of Δf_i, the more robust the solution is, because the same variation of uncertainties leads to a smaller change in the objective function. However, for practical engineering problems, the ASR is always irregular and asymmetric, which means that obtaining the actual area of the ASR is difficult. Therefore, the sensitive direction s_i is used to evaluate the ASR quantitatively. For example, as illustrated in Fig. 1, the change rate of Δf_i is the smallest in the s_1 direction, which indicates that the objective function is less sensitive to variations in uncertainty as compared with other directions. The change rate of Δf_i is the largest in the s_2 direction, indicating the most sensitive direction of the objective to variations in uncertainty.

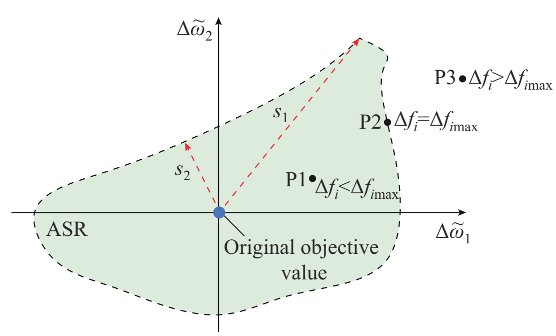

Fig. 1. ASR and sensitive directions.

To estimate the ASR for alleviating computational burden, the concept of a worst-case sensitivity region (WCSR) is introduced. WCSR is defined as the largest n-sphere within the ASR [25] in Fig. 3. No solution within the WCSR affects the feasibility of the SOP allocation decisions, and this robust assessment does not require presumed probability distributions for any uncertainty parameter.

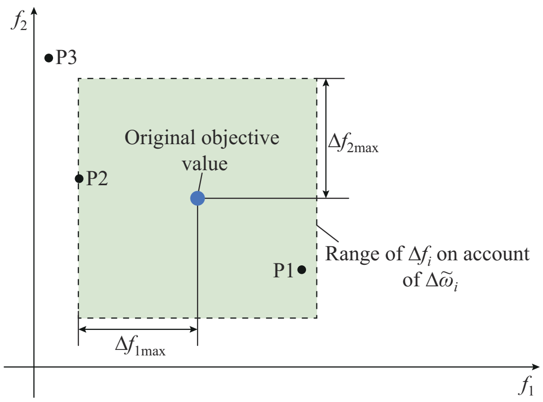

Fig. 2. Range of Δf_i derived from $\Delta\tilde{\omega}_i$.

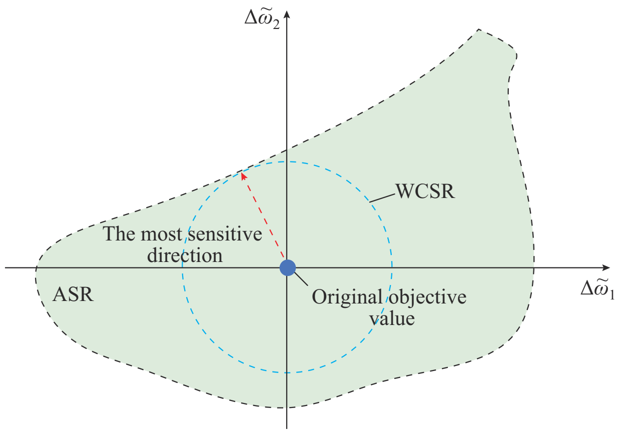

Fig. 3. WCSR.

Because of the symmetry of the WCSR, its radius R_W can be used to represent multi-robust optimality against several uncertainties, which is expressed as:

$$\min_{\Delta\tilde{\omega}} R_W(\Delta\tilde{\omega}) = \left(\sum_{n}^{N_u} \left|\Delta\tilde{\omega}_n\right|^p\right)^{\frac{1}{p}} \tag{1}$$

s.t.

$$\max_{i=1,2,\ldots,N_f} \left|\Delta f_i - \Delta f_{0,i}\right| \le \tau_i^f \tag{2}$$

$$\Delta f_i = f_i(x_0, u_0, \tilde{w}_0 + \Delta\tilde{\omega}) - f_i(x_0, u_0, \tilde{w}_0) \tag{3}$$

where $\Delta f_{0,i}$ is an acceptable deviation; $\Delta\tilde{\omega}$ is the variation in uncertainty; $f_i(x_0, u_0, \tilde{w}_0)$ is the nominal value of objective i, and x_0, u_0, and $\tilde{w}_0$ are the nominal values of the decision, state, and uncertainty variables, respectively; p is a constant that defines R_W as the L_p-norm; τ_i^f is the tolerance for an acceptable deviation $\Delta f_{0,i}$; N_u is the number of uncertainties; and N_f is the number of objective functions.

Although R_W is effective at estimating the ASR, judging whether a solution is sufficiently robust using R_W alone remains difficult. Therefore, a reference robust radius is introduced and determined using an acceptable uncertainty vector. The robustness index F_R is proposed to quantitatively evaluate the robust optimality of the SOP allocation decisions under multiple uncertainties.

$$F_R = R_{ref}/R_W \tag{4}$$

where R_{ref} is the reference robust radius that represents the smallest acceptable radius. Therefore, any R_W smaller than R_{ref} should be considered insufficiently robust.

Incorporating the proposed robustness index in the optimization model as an objective is straightforward but not perfect. On one hand, an additional objective increases the computational burden and difficulty in convergence. On the other hand, F_R is closely related to other technical indices individually instead of collectively. Alternatively, this paper proposes the following indices to incorporate robustness assessment into different technical indices to maintain the number of objectives and directly correlate the robustness assessment with individual technical objectives.

B. Robust Voltage Offset Index

Based on the robustness index previously introduced, a robust voltage offset index F_{offset}^R is proposed to minimize the voltage fluctuations and optimize the operating conditions.

$$\begin{cases} F_{offset}^R = F_R F_{offset} \\ F_{offset} = \sum\limits_{t=1}^{T} \sum\limits_{i=1}^{\Omega_{node}} \left| \dfrac{U_i^t}{U_N} - 1 \right| \end{cases} \tag{5}$$

where F_{offset} is the conventional voltage offset index; Ω_{node} is the number of nodes; U_N is the rated voltage; U_i^t is the voltage of node i at time t; and T is the number of time periods.

C. Robust SOP Utilization Index

Robust SOP utilization index F_{SOP}^R is designed to maximize the utilization of the planned SOP under the same allocation capacity, further reducing the total cost of the distribution network.

$$\begin{cases} F_{SOP}^R = F_R F_{SOP} \\ F_{SOP} = \sum\limits_{t=1}^{T} \sum\limits_{i=1}^{\Omega_{node}} \dfrac{1}{n_{SOP} S_{VSC}} \Bigg(\sqrt{(P_{i,VSC1}^t)^2 + (Q_{i,VSC1}^t)^2} + \\ \qquad \sqrt{(P_{j,VSC2}^t)^2 + (Q_{j,VSC2}^t)^2} \Bigg) \end{cases} \tag{6}$$

where F_{SOP} is the normal SOP utilization index; $P_{i,VSC1}^t$, $P_{j,VSC2}^t$, $Q_{i,VSC1}^t$, and $Q_{j,VSC2}^t$ are the active and reactive power injections of voltage source converters (VSCs) 1 and 2 at nodes i and j at time t, respectively; n_{SOP} is the number of VSC units in the SOP module; and S_{VSC} is the capacity of a single VSC unit.

D. Voltage Collapse Proximity Index (VCPI)

Line-based voltage collapse proximity index $VCPI_l$ is adopted to assess the line voltage stability in failure scenarios based on the concept of maximum power transferable through a line [26]. F_{vcpi} can reveal the effects of an SOP on the voltage stability of a distribution network under fault conditions.

$$\min F_{vcpi} = \sum_{l=1}^{\Omega_{branch}} VCPI_l \tag{7}$$

s.t.

$$VCPI_l = P_l^r / P_l^{r,\max} = Q_l^r / Q_l^{r,\max} \tag{8}$$

$$\begin{cases} P^{r,\max}=\dfrac{(V^s)^2}{Z^s}\dfrac{\cos\varphi}{4\cos^2((\psi-\varphi)/2)} \\ Q^{r,\max}=\dfrac{(V^s)^2}{Z^s}\dfrac{\sin\varphi}{4\cos^2((\psi-\varphi)/2)} \end{cases} \tag{9}$$

where Ω_{branch} is the number of branches; P_l^r and Q_l^r are the active and reactive power transferred to the receiving end though line l in fault scenarios, respectively; ψ and φ are the phase angles of the load and line impedance, respectively; $P^{r,\max}$ and $Q^{r,\max}$ are the maximum active and reactive power transferred at the receiving-end bus, respectively; Z^s is the impedance of the sending-end bus; and V^s is the voltage of the sending-end bus.

III. Multi-stage Robust Optimization Model

A. Framework of Multi-stage Robust Optimization Model

A multi-stage robust optimization model of an SOP in a PV-penetrated distribution network is established, as shown in Fig. 4.

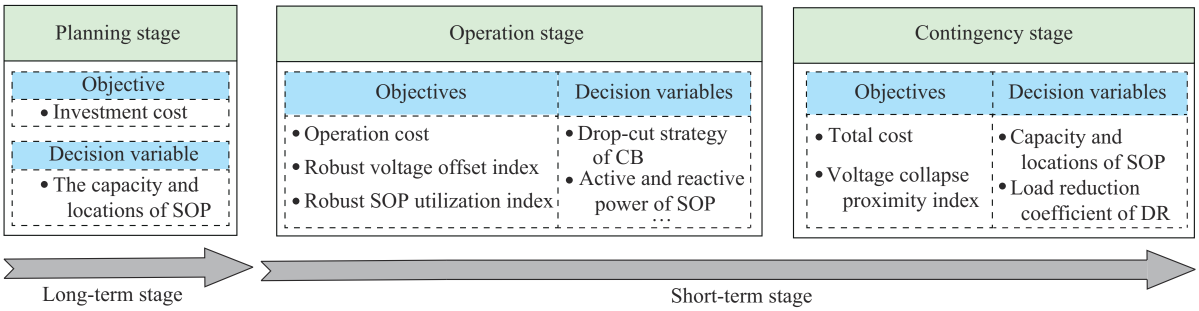

Fig. 4. Multi-stage robust optimization model of SOP.

The first stage is the planning stage, in which the decision variables denote the capacity and locations of the SOP. This is the long-term stage that considers the annual investment cost. The second stage is the normal operation stage, in which the decision variables are the output power of the PV, drop-cut strategy of the CB, active and reactive power of the SOP, active power purchased from the upper substation, and other factors that simulate the actual working conditions of the ADNs. In the third stage, the voltage instability is considered to derive from unexpected contingencies. In this paper, the VCPI is selected to assess the voltage stability, and an SOP coordinated with DR is implemented as a defensive control. The operation and contingency stages are short-term that consider the total cost, robust technical indices, and VCPI.

B. Normal Scenarios

1) Compact Model

The first and second stages aim to minimize the investment cost C_I and operation cost C_O and to optimize the robust technical indices, thereby optimizing the operation conditions in normal scenarios. The specific objective functions are as follows:

$$\min F_1=\{C_I+C_O, F_{offset}^R, F_{SOP}^R\} \tag{10}$$

s.t.

$$g_1(x_1,y_1)=0 \tag{11}$$

$$h_1(x_1,y_1)\leq 0 \tag{12}$$

where F_1 is the objective, which extends to (13) and (29)-(31); x_1 and y_1 are the decision and dependent variables, respectively; g_1 represents the equality constraints, which extend to (1)-(6), (14)-(18), (24)-(26), and (32)-(36); and h_1 represents the inequality constraints, which extend to (19)-(23), (27), (28), and (37).

2) Planning Stage

1) Objective function

The first stage aims to minimize investment costs. The specific objective functions are as follows:

$$\min C_I=C_{SOP,I}+C_{CB,I} \tag{13}$$

① Investment cost of SOP

The investment cost of the SOP can be expressed as:

$$C_{SOP,I}=\frac{r(1+r)^y}{(1+r)^y-1}\sum_{i,j\in n_{SOP}}(c_p x_i+c_p x_j) \tag{14}$$

where r is the discount rate; y is the service life of the VSC; c_p is the annual investment cost per kVA converter power of the VSC; and x_i and x_j are the power capacities of the two VSCs corresponding to the SOP.

② Investment cost of CB

The investment cost of the CB can be expressed as:

$$C_{CB,I}=\frac{r(1+r)^y}{(1+r)^y-1}\sum_{i\in n_{CB}}c_{CB}x_{i,CB} \tag{15}$$

where $x_{i,CB}$ is the power capacity of the CB installed at node i; and c_{CB} is the annual investment cost per kVA of the CB.

2) Constraints

① Constraints of the SOP

The SOP is installed between adjacent feeders in the ADNs, as shown in Fig. 5.

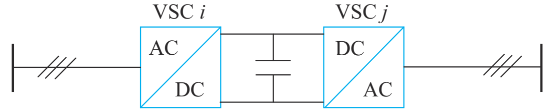

Fig. 5. Modeling of SOP.

The SOP power equation at time t can be expressed as:

$$P_{i,VSC1}^t+P_{j,VSC2}^t+P_{i,VSC1}^{L,t}+P_{j,VSC2}^{L,t}=0 \tag{16}$$

$$P_{i,VSC1}^{L,t}=A_{VSC1}\sqrt{(P_{i,VSC1}^t)^2+(Q_{i,VSC1}^t)^2} \tag{17}$$

$$P_{j,VSC2}^{L,t} = A_{VSC2}\sqrt{(P_{j,VSC2}^{t})^2 + (Q_{j,VSC2}^{t})^2} \tag{18}$$

$$Q_{VSC1\min} \le Q_{VSC1}^{t} \le Q_{VSC1\max} \tag{19}$$

$$Q_{VSC2\min} \le Q_{j,VSC2}^{t} \le Q_{VSC2\max} \tag{20}$$

$$\sqrt{(P_i^t)^2 + (Q_i^t)^2} \le n_{sop} S_{VSC} \tag{21}$$

$$\sqrt{(P_j^t)^2 + (Q_j^t)^2} \le n_{sop} S_{VSC} \tag{22}$$

where P_i^t, P_j^t, Q_i^t, and Q_j^t are the active and reactive power injections of nodes i and j in the ADNs, respectively; $P_{i,VSC1}^{L,t}$ and $P_{j,VSC2}^{L,t}$ are the power losses of VSCs 1 and 2 at nodes i and j, respectively; A_{VSC1} and A_{VSC2} are the power loss coefficients; and $Q_{VSC1\min}$, $Q_{VSC1\max}$, $Q_{VSC2\min}$, and $Q_{VSC2\max}$ are the minimum and maximum reactive power injections of VSC1 and VSC2, respectively.

Equation (16) represents the active power balance of the SOP; (17) and (18) are the power-loss equations of the VSC; (19) and (20) represent the reactive power injection constraints of the SOP; and (21) and (22) represent the capacity constraints of the VSC.

② Upper limits of VSC units

$$0 \le n_{sop} \le n_{sop\max} \tag{23}$$

where $n_{sop\max}$ is the upper limit of the number of VSC units of the SOP.

③ Linearized DistFlow equations

The following power flow equations should be satisfied [27]:

$$\begin{cases} \sum\limits_{i \in u(j)} (P_{ij,t} - P_{ij}^{L,t}) + P_j^t = \sum\limits_{k \in v(j)} P_{jk}^t \\ \sum\limits_{i \in u(j)} (Q_{ij,t} - Q_{ij}^{L,t}) + Q_j^t = \sum\limits_{k \in v(j)} Q_{jk}^t \\ P_j^t = P_{j,PV}^t + P_{j,VSC2}^t - P_{j,Load}^t \\ Q_j^t = Q_{j,PV}^t + Q_{j,VSC2}^t + Q_{j,CB}^t - Q_{j,Load}^t \end{cases} \tag{24}$$

$$U_j^t = U_i^t - (r_{ij} P_{ij,t} + x_{ij} Q_{ij,t})/U_N \tag{25}$$

$$\begin{cases} P_{ij}^{L,t} = r_{ij}(P_{ij,t}^2 + Q_{ij,t}^2)/U_N^2 \\ Q_{ij}^{L,t} = x_{ij}(P_{ij,t}^2 + Q_{ij,t}^2)/U_N^2 \end{cases} \tag{26}$$

where r_{ij} is the resistance value of branch ij; x_{ij} is the reactance value of branch ij; $i \in u(j)$ represents that node i is subordinate to the set $u(j)$ of parent nodes connected to node j; $k \in v(j)$ represents that node k is subordinate to the set $v(j)$ of child nodes connected to node j; $P_{ij,t}$ and $Q_{ij,t}$ are the active and reactive power on branch ij at time t, respectively; $P_{ij}^{L,t}$ and $Q_{ij}^{L,t}$ are the active and reactive power losses on branch ij, respectively; P_j^t and Q_j^t are the active and reactive power injections into node j, respectively (node j is selected in this case as a substitute for other nodes, excluding the balanced one); $P_{j,PV}^t$ and $Q_{j,PV}^t$ are the active and reactive power injections of distributed power supply PV, respectively; $P_{j,Load}^t$ and $Q_{j,Load}^t$ are the active and reactive power injections of the load, respectively; $Q_{j,CB}^t$ is the reactive power of the CB; U_j^t is the voltage of node j at time t; and U_N is the system-rated voltage.

④ Network operation constraints

The node voltage and branch active power must satisfy the following constraints to ensure safe operation of the system:

$$\begin{cases} U_{j,\min} \le U_j^t \le U_{j,\max} \\ 0 \le P_{ij,t} \le P_{ij,\max} \end{cases} \tag{27}$$

where $U_{j,\min}$ and $U_{j,\max}$ are the minimum and maximum node voltages, respectively; $P_{ij,t}$ is the active power of branch ij; and $P_{ij,\max}$ is the maximum branch active power.

⑤ CB switching constraints

$$\begin{cases} Q_{j,CB}^t = n_{i,CB} Q_{\text{step}}^{CB} \\ n_{i,CB} \le x_{i,CB} \\ B_{i,t}^{CB} Q_{\text{step}}^{CB} \le \left| Q_{j,CB}^{t+1} - Q_{j,CB}^t \right| \le B_{i,t}^{CB} Q_{\text{step}}^{CB} x_{i,CB} \\ \sum\limits_{t=1}^{T-1} B_{i,t}^{CB} \le B_{CB\max} \end{cases} \tag{28}$$

where $n_{i,CB}$ is the number of CBs in operation; Q_{step}^{CB} is the capacity of the CB per unit; $B_{i,t}^{CB}$ is the binary variable if the CB is in operation, in which case $B_{i,t}^{CB} = 1$; otherwise, $B_{i,t}^{CB} = 0$; and $B_{CB\max}$ is the maximum switching times of the CB.

3) Normal Operation Stage

The operation cost includes the power exchange cost, SOP operation cost, loss cost of the VSC converter, CB drop-cut cost, network loss, and emission cost. The technical indices include the robust offset voltage index and robust SOP utilization index.

1) Objective function

$$\min C_O = C_{SOP,O} + C_{CB,O} + C_{loss1} + C_{loss2} + C_E \tag{29}$$

$$\min F_{offset}^R \tag{30}$$

$$\min \frac{1}{F_{SOP}^R} \tag{31}$$

① SOP operation cost

$$C_{SOP,O} = \alpha \sum_{i,j \in n_{SOP}} p_s c_{SOP,I} S_{i,j,SOP} D_y \tag{32}$$

where α is the annual SOP operation cost coefficient; $c_{SOP,I}$ is the investment cost of the SOP per apparent power; D_y is the number of days in a year adopted to convert the daily cost into the annual cost; and $S_{i,j,SOP}$ is the capacity of the SOP on branch ij.

② CB drop-cut cost

$$C_{CB,O} = \sum_{t \in T} \sum_{i,j \in \Omega_{line}} c_{CB,O} B_{i,t}^{CB} \tag{33}$$

where $c_{CB,O}$ is the CB drop-cut cost.

③ Network loss cost

$$C_{loss1} = \sum_{t \in T} \sum_{i,j \in \Omega_{line}} c_{loss1} r_{ij} D_y (P_{ij,t}^2 + Q_{ij,t}^2)/U_N^2 \tag{34}$$

where c_{loss1} is the daily network loss cost.

④ Converter loss cost

$$C_{loss2} = \sum_{t \in T} \sum_{i,j \in \Omega_{line}} c_{loss2} (P_{i,VSC1}^{L,t} + P_{j,VSC2}^{L,t}) D_y \tag{35}$$

where c_{loss2} is the daily converter loss cost.

⑤ Emission cost

Because the PV does not generate carbon emissions, the carbon cost in this study is generated by the upper grid.

$$C_E=\sum_{t=1}^{T}\eta c_{emis}P_{sub,t}D_y \tag{36}$$

where c_{emis} is the daily emission cost; $P_{sub,t}$ is the active power obtained from the upper substation; and η is the carbon emission intensity per kWh for the upper substation.

2) Constraints

In addition, to satisfy constraints (16)-(28), PV generation constraints must also be satisfied.

$$\begin{cases} 0\le P_{j,PV}^{t}\le P_{j,PV}^{\max} \\ Q_{j,PV}^{t}=P_{j,PV}^{t}\tan\varphi_{PV} \end{cases} \tag{37}$$

where $P_{j,PV}^{\max}$ is the maximum available active power of the PV units; and φ_{PV} is the power factor angle of the PV.

C. Contingency Scenarios

1) Compact Model

With unexpected contingencies in ADNs, the voltage collapse proximity index is a major index for assessing the voltage stability. In this case, the DR and SOP are used to ensure voltage stability. Accordingly, the objectives of the contingency scenario stage can be expressed as:

$$\min F_2=\{F_{vcpi},C_{total}\} \tag{38}$$

$$C_{total}=C_{DR}+C_{SOP,I}+C_{SOP,O}+C_{loss1}+C_{loss2}+C_E \tag{39}$$

s.t.

$$g_2(x_2,y_2)=0 \tag{40}$$

$$h_2(x_2,y_2)\le 0 \tag{41}$$

where F_2 is the objective, which extends to (7)-(9) and (39); x_2 and y_2 are the decision and dependent variables, respectively; g_2 denotes the equality constraints, which extend to (16)-(18), (39), (42)-(44), and (46)-(48); and h_2 denotes the inequality constraints, which extend to (19)-(23), (27), (28), and (37).

2) Contingency Stage

1) Objective function

The load reduction cost is expressed as:

$$C_{DR}=\sum_{t=1}^{T}\sum_{i\in A_{DR}}c_{DR}P_{j,Load}^{t}\lambda_{i,t} \tag{42}$$

where c_{DR} is the load-cut cost per kWh; $\lambda_{i,t}$ is the load reduction coefficient; and A_{DR} is the node set of the DR.

2) Constraints

In addition to constraints (16)-(23), (27), (28), and (37), the DR constraints must also be satisfied.

① DR constraints

$$\begin{cases} \Delta P_j^t=\lambda_{i,t}P_{j,Load}^t \\ \Delta Q_j^t=\lambda_{i,t}Q_{j,Load}^t \end{cases} \tag{43}$$

$$\begin{cases} P_{j,Load,DR}^t=P_{j,Load}^t-\Delta P_{i,t} \\ Q_{j,Load,DR}^t=Q_{j,Load}^t-\Delta Q_{i,t} \end{cases} \tag{44}$$

$$\lambda_{\min}\le\lambda_{i,t}\le\lambda_{\max} \tag{45}$$

where ΔP_j^t and ΔQ_j^t are the active and reactive power reductions, respectively; $\lambda_{\min}$ and $\lambda_{\max}$ are the minimum and maximum load reduction coefficients, respectively; and $P_{j,Load,DR}^t$ and $Q_{j,Load,DR}^t$ are the active and reactive power injections of load following load reduction, respectively.

② New linearized DistFlow equations

$$\begin{cases} \sum_{i\in u(j)}(P_{ij,t,s}-P_{ij}^{L,t,s})+P_j^{t,s}=\sum_{k\in v(j)}P_{jk}^{t,s} \\ \sum_{i\in u(j)}(Q_{ij,t,s}-Q_{ij}^{L,t,s})+Q_j^{t,s}=\sum_{k\in v(j)}Q_{jk}^{t,s} \\ P_j^{t,s}=P_{j,PV}^{t,s}+P_{j,VSC2}^{t,s}-P_{j,Load,DR}^{t,s} \\ Q_j^{t,s}=Q_{j,PV}^{t,s}+Q_{j,VSC2}^{t,s}+Q_{j,CB}^{t,s}-Q_{j,Load,DR}^{t,s} \end{cases} \tag{46}$$

$$U_j^{t,s}=U_i^{t,s}-(r_{ij}P_{ij,t,s}+x_{ij}Q_{ij,t,s})/U_N \tag{47}$$

$$\begin{cases} P_{ij}^{L,t,s}=r_{ij}(P_{ij,t,s}^2+Q_{ij,t,s}^2)/U_N^2 \\ Q_{ij}^{L,t,s}=x_{ij}(P_{ij,t,s}^2+Q_{ij,t,s}^2)/U_N^2 \end{cases} \tag{48}$$

IV. Computational Steps

The single-objective model optimization method (Cplex [28] in this paper) and multi-objective model optimization method (NSGA-II [29] in this paper) are coordinated to solve this multi-stage optimization problem. A computational flow of the proposed method is shown in Fig. 6. The computational steps are as follows.

A. Planning Stage (Main Program Solved by NSGA-II)

Step 1: initialization. After the algorithm parameters are set, the first generation of the population is initialized, including decision variables for the SOP, CB installation, and output power of the PV.

Step 2: coordination of planning and contingency stages. The method used in this step involves contingency determination. Power flow calculations are conducted to determine whether contingencies occur in the ADNs. Provided no contingency occurs, we can proceed to *Step 3*. Otherwise, defensive controls should be implemented and the subroutine should be booted (*Step 9*).

Step 3: objective calculation. The total cost and robust technical indices are calculated to optimize the capacities and sites of SOPs.

Step 4: individual update. Identify and renew the best individuals of the present generation, including non-dominated sorting, crowding distance and fitness calculation, selection, crossover, and mutation implemented by NSGA-II.

Step 5: coordination of planning and operation stage. The method for this step is as follows: either reaching the maximum number of iterations or finding no other new non-dominated solution in a predefined number of successive iterations to determine the evaluation condition for booting the operation-stage subroutine. Otherwise, proceed to the next iteration.

Step 6: update the optimization capacity and sites of SOP. The fuzzy membership function is adopted to determine the optimal capacity and sites of the SOP. After the conditions for *Step 5* are met, the main procedure terminates and the optimization for the operation stage commences (*Step 7*) with the optimal capacity and sites of the SOP imported.

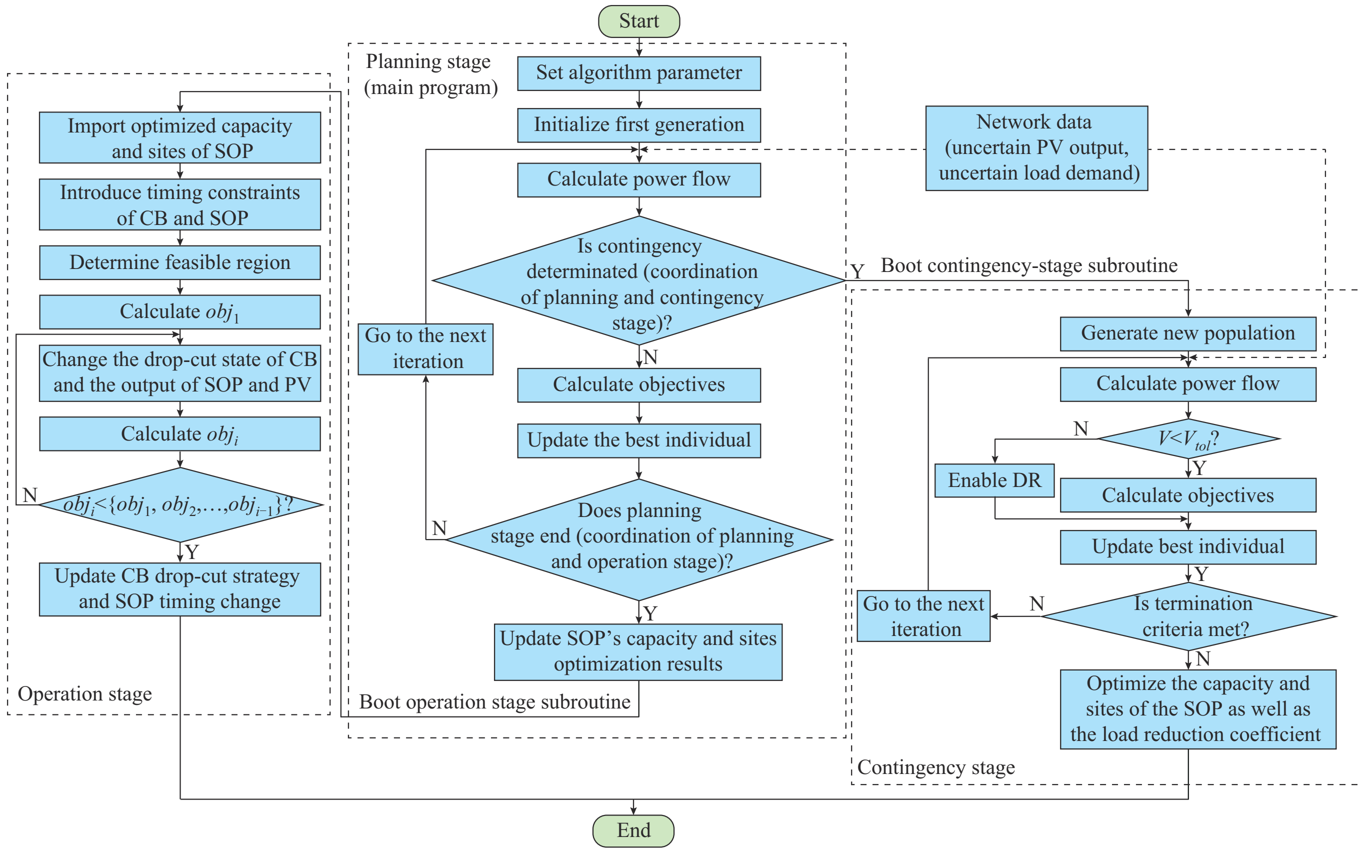

Fig. 6. Computational flow of proposed method.

B. Operation Stage (Solved by Cplex)

Step 7: determine the feasible region. The feasible region is formed by constraints (1)-(6), (14)-(24), (26)-(28), and (32)-(37).

Step 8: update the CB drop-cut strategy and SOP timing change. The CB drop-cut strategy and the active and reactive power support from the SOP are optimized by Cplex.

C. Contingency Stage (Solved by NSGA-II)

Step 9: generate a new population. The first generation of population in the planning stage is overridden by the decision variables for the SOP, the DR (enabled when the voltage exceeds the threshold), and the output power of the PV following contingency determination.

Step 10: objective calculation. The total cost and VCPI are calculated to optimize the capacity and sites of the SOP as well as the load reduction coefficient.

Step 11: termination criteria. The procedure terminates when the termination criteria of Cplex or NSGA-II are satisfied.

V. Case Studies

A. Modified IEEE 33-node Distribution System

The modified IEEE 33-node distribution system is illustrated in Fig. 7. The system parameters can be found in [30]. The unit capacity of each VSC is 50 kVA, and the power loss coefficient of the VSC is 0.02 [13]. The capacity of the PV converter is 800 kVA [7], the voltage limits are [0.95, 1.05]p.u., and the network loss cost is 0.5 \$/kWh [13]. The maximum number of installed VSCs in each ADN is assumed to be 10 units. The candidate installation locations of the SOP units are the tie-line switches, which are connected between the buses (i.e., (8)-(21), (9)-(15), (12)-(22), (18)-(33), and (25)-(29)) [4], as shown in Fig. 7. The candidate locations of CBs are buses 24 and 30. Each CB installation node is equipped with 10 groups of capacitors, each with a capacity of 50 kvar, and the maximum switching times are 5 per day. The demand response load shedding nodes are 7, 10, 13, 17, and 23, with a load shedding factor ranging from 0 to 0.2. The DR load shedding price is 1 \$/kWh, and the candidate locations for the five PVs are shown in Fig. 7.

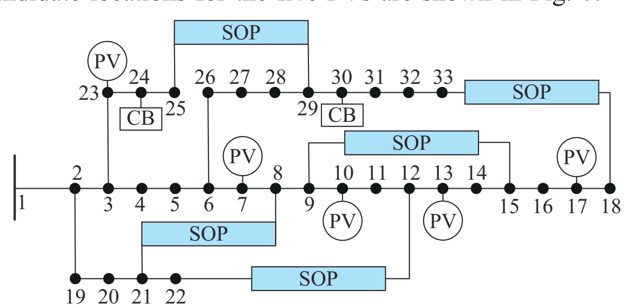

Fig. 7. Modified IEEE 33-node distribution system.

B. Numerical Results and Discussion

For a detailed analysis and discussion, the robust SOP utilization index is converted to its reciprocal, $1/F_{SOP}^{R}$. The smaller the value of all objectives, the more optimal the results are.

1) Simulation Results and Comparison Study of Normal Stage

A Pareto front with 10 robust Pareto optimal solutions of the proposed method is shown in Fig. 8. The fuzzy membership function [31] is used to select the final optimal solution, as illustrated in Table I.

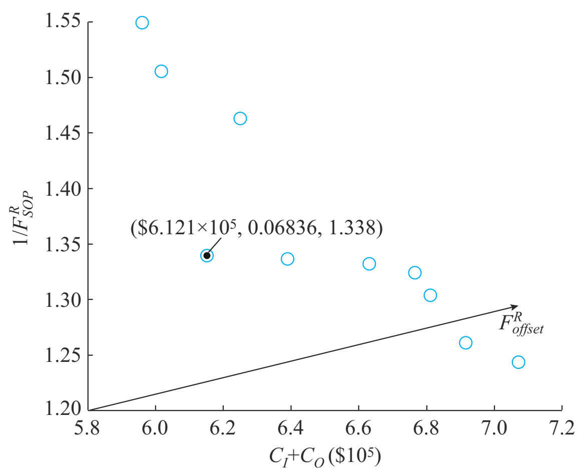

Fig. 8. Pareto front with 10 robust Pareto optimal solutions of proposed method.

TABLE I
VALUES OF INDICES OF FINAL OPTIMAL SOLUTION

C_I+C_O ($)	F^R_{offset}	$1/F^R_{SOP}$	F^R_{SOP} (%)
612101.97	0.07	1.34	74.74

The capacities of the SOP of the final optimal solution are shown in Table II.

TABLE II
CAPACITIES OF SOP OF FINAL OPTIMAL SOLUTION

Location	Capacity (kVA)
12-22	100
8-21	100
9-15	100
18-33	150
25-29	100

Three cases are selected to investigate the effects of SOPs and CB on voltage stability and network loss.

1) Case 1: PV-penetrated ADNs without SOPs or CB installation.

2) Case 2: PV-penetrated ADNs with CB installation only.

3) Case 3: PV-penetrated ADNs with SOPs and CB installation.

Figure 9 shows the voltage profiles for the three cases. Case 3 has the smallest voltage offset and fluctuation range as compared with the other cases, where the fluctuation range is [0.955, 1.01]p. u.. This finding indicates that the SOP can provide a certain amount of reactive power, which can be coordinated with the CB to support the voltage of the ADNs and significantly improve the voltage profile.

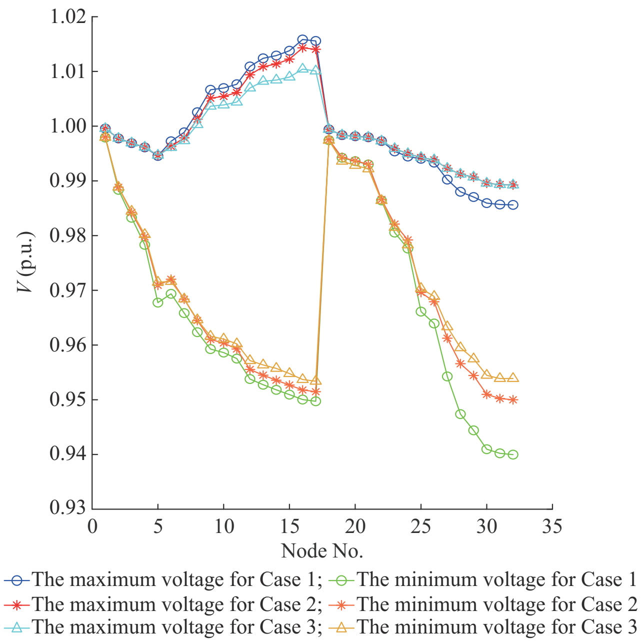

Fig. 9. Voltage profiles for three cases.

Table III presents the loss costs for the three cases. As can be observed, Case 3 reduced the network loss by 12.4% as compared with Case 2 and by 29.3% as compared with Case 1, revealing that the SOP improved the power profile among feeders and decreased the network loss. Compared with the single reactive optimization measure (i.e., the CB in this paper) in Case 2, Case 3 adds the active power regulation of the SOP to improve the power profile, thus minimizing the network loss further onwards.

TABLE III
LOSS COSTS FOR THREE CASES

Case	Loss cost ($)
1	146150.171
2	117982.442
3	103317.219

Table IV illustrates a comparison of emission costs for the three cases derived from power purchase from the upper grid. Case 1 has the highest emission cost as compared with Cases 2 and 3. This result is mostly due to the existence of fewer active control methods and the higher uncertainty of the PV output in Case 1. This results in more power purpurchase and emission costs, indicating that the coordinated allocation of the SOP and CB could reduce carbon emissions by helping DGs integrate and decrease power purchase.

2) Comparison of Contingency Stages

This paper presumes that branch 32-33 and branch 3-23 have contingencies in the modified IEEE 33-node system, as shown in Fig. 10. Three cases are selected to investigate the effects of SOP and DR allocation on voltage stability when a contingency occurs.

1) Case 4: ADNs with only DR allocation to avoid voltage instability.

2) Case 5: ADNs with only SOP allocation to avoid voltage instability.

3) Case 6: ADNs with coordinated SOP and DR allocation to avoid voltage instability.

TABLE IV
EMISSION COSTS FOR THREE CASES

Case	Emission cost ($)
4	597610
5	595420
6	595360

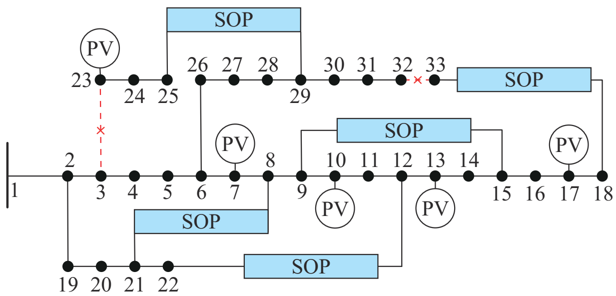

Fig. 10. Modified IEEE 33-node distribution network of contingency stage.

The Pareto optimal solutions for the three cases are compared in Fig. 11. The fuzzy membership function [31] was used to select the final optimal solution, as listed in Table V. The SOP capacities of the three cases are shown in Table VI. The load DR situations of the three cases are listed in Table VII.

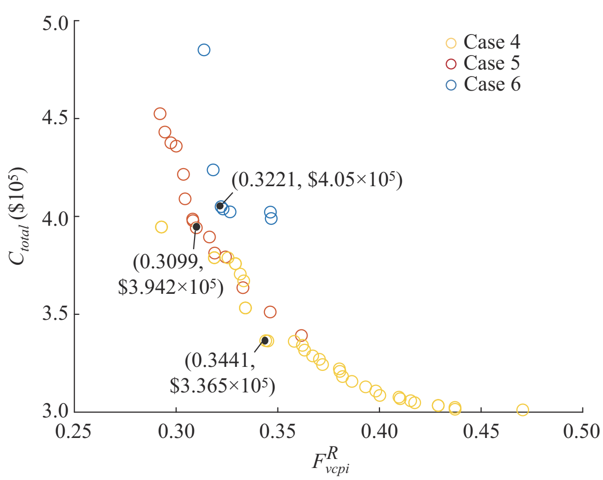

Fig. 11. Comparison of Pareto optimal solutions for three cases.

TABLE V
INDEX VALUES OF CONTINGENCY STAGE OF THREE CASES

Case	VCPI	Cost ($)
4	0.3463	337500
5	0.3339	475000
6	0.2812	365700

As shown in Tables V and VI, although Case 6 allocates a greater number of SOPs than Case 5, the cost for Case 6 exhibites a 23% reduction, and the VCPI has a 15.8% reduction compared with Case 5, indicating that coordinated allocation of an SOP and DR has better economic performance and voltage stability than installing only one SOP. Case 4 has a lower cost than Case 6 due to the absence of SOPs. The bus VCPI of Case 4 is higher than that of Case 6, meaning that Case 4 is more prone to voltage collapse under worse contingencies. Figure 12 also indicates that Case 4 has a greater voltage fluctuation range compared with Case 6. In addition, the network loss of Case 6 is $135250, whereas that of Case 4 is $451590. Table VII reveals that less load reduction is required after an SOP is introduced into the ADNs. Therefore, the coordinated allocation of the SOP and DR could effectively reduce network loss and improve the voltage profile under contingencies.

TABLE VI
SOP CAPACITIES OF THREE CASES

Location	Capacity (kVA)		
	Case 4	Case 5	Case 6
12-22		100	50
8-21		150	200
9-15		100	150
18-33		100	150
25-29		300	300

TABLE VII
LOAD DR SITUATIONS OF THREE CASES

Location	$\lambda_{i,s,t}$		
	Case 4	Case 5	Case 6
7	0.101		0.092
10	0.123		0.110
13	0.093		0.093
17	0.155		0.070
23	0.155		0.113

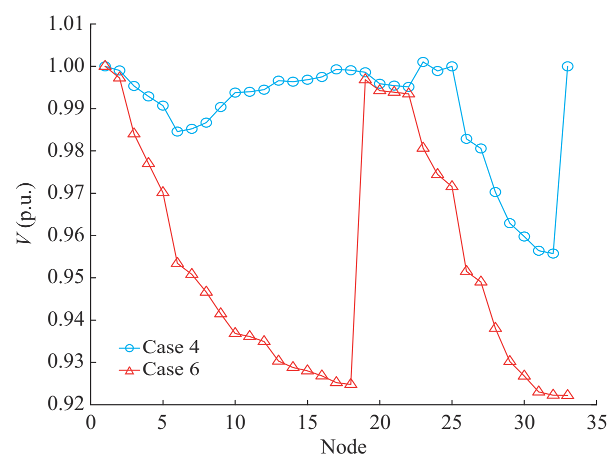

Fig. 12. Comparison of voltage profile for Cases 4 and 6.

C. Comparison Study of Effects of Robustness Index

Two cases are selected to investigate the effects of the robustness index.

1) Case 7: F_{offset} and F_{SOP} are used to evaluate the perfor-

mance of the normal operation stage.

2) Case 8: F_{offset}^R and F_{SOP}^R are used to evaluate the performance of the normal operation stage.

The Pareto optimal solutions for Cases 7 and 8 are compared in Fig. 13. Although the value of the robust index might not be strictly optimal, the robust optimality of the robust Pareto solution can be improved against the uncertainties of load demand and PV, making the optimal allocation results of the SOP and CB more effective.

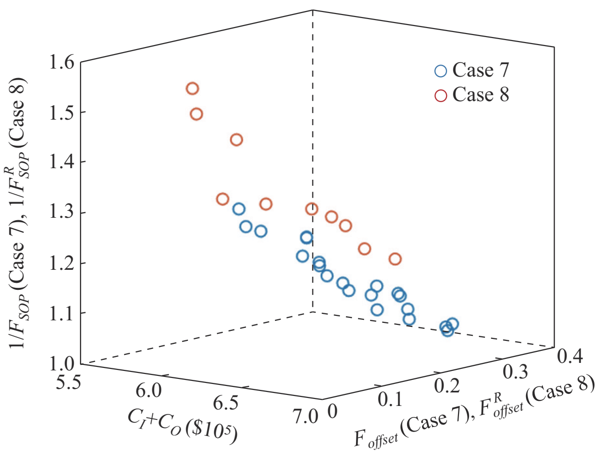

Fig. 13. Comparison of Pareto optimal solutions for Cases 7 and 8.

In addition, a robustness analysis does not require assumptions about the probability distribution of uncertain variables, which reduces the adverse effects of uncertainties. Under practical operating conditions, the fluctuations of the PV and load deviate from the set value of the planning scenarios. With a typical solution on the Pareto fronts as an example and based on the assumption that $\tilde{w}_n$ has an error of ±0.2, F_{offset} worsenes from 0.10 to 0.84, and the SOP utilization becomes increasingly inadequate from 57.9% to 51.2% in Case 7. By contrast, F_{offset}^R increases from 0.10 to 0.79, whereas the SOP utilization decreases from 72.1% to 71.3% in Case 8, indicating that the proposed quantitative robustness assessment could make the objective function less sensitive and more optimal to variations in uncertainty.

D. Comparison Study of Effects of SOP Utilization Index

Two cases are selected to investigate the effects of the SOP utilization index.

1) Case 9: F_{offset}^R and cost are used to determine the optimal allocated SOP capacity without considering F_{SOP}^R.

2) Case 10: F_{offset}^R, F_{SOP}^R, and cost are used to determine the optimal allocated SOP capacity.

The fuzzy membership function [31] is used to select the final optimal solution of the two cases, the index values for which could be found in Table VIII. The SOP capacities of the two cases are listed in Table IX. As shown in Table VIII, the SOP utilization in Case 10 is 19.57% higher than that of Case 9, whereas the cost and robust voltage offset index decrease by 7.84% and 50%, respectively, after F_{SOP}^R is considered. Table IX shows that the capacity of the SOP planning for Case 9 is less than that of Case 10, resulting in a worse power adjustment ability and in turn increasing network loss and voltage fluctuation. Thus, the comparison study reveals that the robust SOP utilization index could effectively improve both the SOP utilization and the operation level while reducing the total cost.

TABLE VIII
INDEX VALUES OF NORMAL STAGE BETWEEN TWO CASES

Case	C_I+C_O (\$)	F_{offset}^R	$1/F_{SOP}^R$	F_{SOP}^R (%)
Case 9	664194.91	0.14	1.81	55.19
Case 10	612101.97	0.07	1.34	74.74

TABLE IX
SOP CAPACITIES BETWEEN TWO CASES

Location	Capacity (kVA)	
	Case 9	Case 10
12-22	100	100
8-21	100	100
9-15	50	100
18-33	50	150
25-29	50	100

VI. CONCLUSION

This paper proposes a multi-stage coordinated optimization for the SOP allocation in ADNs with PV based on robust technical indices to enhance the effectiveness and robust optimality of the solutions and the SOP utilization. The applicability of the proposed model is verified through case studies. The major conclusions are as follows.

1) The proposed quantitative robustness assessment method could effectively improve the robust optimality and effectiveness of allocation results without requiring assumed probability distributions for uncertain variables.

2) When introducing a robust SOP utilization index, the proposed model could improve the SOP utilization (e.g., by 19.57%) and operation conditions (e.g., voltage offset decreased by 50%) while reducing the investment and operation costs (e.g., by 7.84%).

3) The proposed multi-stage optimization framework and corresponding computational method demonstrated that the introduction of an SOP could adjust the transmitted power and effectively decrease network loss (e.g., by 29.3% compared with no SOP or CB installation), further improving the economy of ADNs. In addition, case studies prove that an SOP can provide reactive power to support the voltage of ADNs in coordination with the CB, thereby enhancing voltage quality. Furthermore, when contingencies occurred, the SOP could reduce both the load demand and voltage collapse risk (e.g., by 18.8% compared with only DR allocation). Thus, the proposed multi-stage allocation model is more comprehensive and sophisticated than the conventional models.

REFERENCES

[1] S. Zhang and J. Yu, "Bayesian deep learning for dynamic power system state prediction considering renewable energy uncertainty," *Journal of Modern Power Systems and Clean Energy*, vol. 10, no. 4, pp. 913-922, Jul. 2022.

[2] Q. Yang, J. Wang, H. Yin *et al*., “A fast calculation method for long-term security-constrained unit commitment of large-scale power systems with renewable energy,” *Journal of Modern Power Systems and Clean Energy*, vol. 10, no. 5, pp. 1127-1137, Sept. 2022.

[3] J. M. Bloemink and T. C. Green, “Increasing distributed generation penetration using soft normally-open points,” in *Proceedings of IEEE PES General Meeting*, Minneapolis, USA, Jul. 2010, pp. 1-8.

[4] V. B. Pamshetti and S. P. Singh, “Coordinated allocation of BESS and SOP in high PV penetrated distribution network incorporating DR and CVR schemes,” *IEEE Systems Journal*, vol. 16, no. 1, pp. 420-430, Mar. 2022.

[5] L. Bai, T. Jiang, F. Li *et al*., “Distributed energy storage planning in soft open point based active distribution networks incorporating network reconfiguration and DG reactive power capability,” *Applied Energy*, vol. 210, pp. 1082-1091, Jan. 2018.

[6] A. Maulik, “Probabilistic power management of a grid-connected microgrid considering electric vehicles, demand response, smart transformers, and soft open points,” *Sustainable Energy, Grids and Networks*, vol. 30, pp. 1-19, Jun. 2022.

[7] C. Lou, J. Yang, E. Vega-Fuentes *et al*., “Multi-terminal phase-changing soft open point SDP modeling for imbalance mitigation in active distribution networks,” *International Journal of Electrical Power & Energy Systems*, vol. 142, pp. 1-9, Nov. 2022.

[8] F. Sun, M. Yu, Q. Wu *et al*., “A multi-time scale energy management method for active distribution networks with multiple terminal soft open point,” *International Journal of Electrical Power & Energy Systems*, vol. 128, no. 4, p. 106767, Jun. 2021.

[9] Z. Liu and L. Wang, “A robust strategy for leveraging soft open points to mitigate load altering attacks,” *IEEE Transactions on Smart Grid*, vol. 13, no. 2, pp. 1555-1569, Mar. 2022.

[10] F. Sun, J. Ma, M. Yu *et al*., “Optimized two-time scale robust dispatching method for the multi-terminal soft open point in unbalanced active distribution networks,” *IEEE Transactions on Sustainable Energy*, vol. 12, no. 1, pp. 587-598, Jan. 2021.

[11] T. Ding, Z. Wang, W. Jia *et al*., “Multiperiod distribution system restoration with routing repair crews, mobile electric vehicles, and soft-open-point networked microgrids,” *IEEE Transactions on Smart Grid*, vol. 11, no. 6, pp. 4795-4808, Nov. 2020.

[12] J. Ding, K. Xie, B. Hu *et al*., “Mixed aleatory-epistemic uncertainty modeling of wind power forecast errors in operation reliability evaluation of power systems,” *Journal of Modern Power Systems and Clean Energy*, vol. 10, no. 5, pp. 1174-1183, Sept. 2022.

[13] P. Li, F. Zhang, X. Ma *et al*., “Operation cost optimization method of regional integrated energy system in electricity market environment considering uncertainty,” *Journal of Modern Power Systems and Clean Energy*, vol. 11, no. 1, pp. 368-380, Jan. 2023.

[14] J. Zhang, A. Foley, and S. Wang, “Optimal planning of a soft open point in a distribution network subject to typhoons,” *International Journal of Electrical Power & Energy Systems*, vol. 129, pp. 1-13, Jul. 2021.

[15] H. Ji, C. Wang, P. Li *et al*., “Robust operation of soft open points in active distribution networks with high penetration of photovoltaic integration,” *IEEE Transactions on Sustainable Energy*, vol. 10, no. 1, pp. 280-289, Jan. 2019.

[16] T. Zhang, J. Wang, H. Zhong *et al*., “Soft open point planning in renewable-dominated distribution grids with building thermal storage,” *CSEE Journal of Power and Energy Systems*, doi: 10.17775/CSEEJPES.2020.03660.

[17] I. Sarantakos, M. Peker, N. M. Zografou-Barredo *et al*., “A robust mixed-integer convex model for optimal scheduling of integrated energy storage – soft open point devices”, *IEEE Transactions on Smart Grid*, vol. 13, no. 5, pp. 4072-4087, Sept. 2022.

[18] I. Sarantakos, N. M. Zografou-Barredo, D. Huo *et al*., “A reliability-based method to quantify the capacity value of soft open points in distribution networks,” *IEEE Transactions on Power Systems*, vol. 36, no. 6, pp. 5032-5043, Nov. 2021.

[19] P. Li, H. Ji, C. Wang *et al*., “Optimal operation of soft open points in active distribution networks under three-phase unbalanced conditions,” *IEEE Transactions on Smart Grid*, vol. 10, no. 1, pp. 380-391, Jan. 2019.

[20] S. Zhang, L. Zhang, K. Li *et al*., “Multi-objective planning of soft open point in active distribution network based on bi-level programming,” in *Proceedings of 2019 IEEE Innovative Smart Grid Technologies*, Chengdu, China, Oct. 2019, pp. 3251-3255.

[21] S. Rezaeian-Marjani, S. Galvani, and V. Talavat, “A generalized probabilistic multi-objective method for optimal allocation of soft open point (SOP) in distribution networks,” *IET Renewable Power Generation*, vol. 16, pp. 1046-1072, Feb. 2022.

[22] Q. Qi, J. Wu, L. Zhang *et al*., “Multi-objective optimization of electrical distribution network operation considering reconfiguration and soft open points,” *Energy Procedia*, vol. 103, pp. 141-146, Dec. 2016.

[23] Z. M. Ali, I. M. Diaaeldin, A. El-Rafei *et al*., “A novel distributed generation planning algorithm via graphically-based network reconfiguration and soft open points placement using Archimedes optimization algorithm,” *Ain Shams Engineering Journal*, vol. 12, pp. 1923-1941, Jun. 2021.

[24] J. Li, S. Ge, S. Zhang *et al*., “A multi-objective stochastic-information gap decision model for soft open points planning considering power fluctuation and growth uncertainty,” *Applied Energy*, vol. 317, pp. 1-11, Jul. 2022.

[25] S. Gunawan and S. Azarm, “Non-gradient based parameter sensitivity estimation for single objective robust design optimization,” *Journal of Mechanical Design*, vol. 126, no. 3, pp. 395, May 2004.

[26] M. Moghavvemi and O. Faruque, “Real-time contingency evaluation and ranking technique,” *IEE Proceedings–Generation Transmission & Distribution*, vol. 145, no. 5, pp. 517-524, Sept. 1998.

[27] C. Zhang, Y. Xu, and Z. Dong, “Robustly coordinated operation of a multi-energy micro-grid in grid-connected and islanded modes under uncertainties,” *IEEE Transactions on Sustainable Energy*, vol. 11, no. 2, pp. 640-651, Feb. 2019.

[28] IBM. (2018, Jun.). ILOG CPLEX optimization studio. [Online]. Available: https://www.ibm.com/products/ilog-cplex-optimization-studio

[29] K. Deb, A. Pratap, S. Agarwal *et al*., “A fast and elitist multi-objective genetic algorithm: NSGA-II,” *IEEE Transactions on Evolutionary Computation*, vol. 6, no. 2, pp. 182-197, Apr. 2002.

[30] D. Tran and A. M. Khambadkone, “Energy management for lifetime extension of energy storage system in micro-grid applications,” *IEEE Transactions on Smart Grid*, vol. 4, no. 3, pp. 1289-1296, Sept. 2019.

[31] S. Agrawal, B. K. Panigrahi, and M. K. Tiwari, “Multi-objective particle swarm algorithm with fuzzy clustering for electrical power dispatch,” *IEEE Transactions on Evolutionary Computation*, vol. 12, no. 5, pp. 529-541, Oct. 2008.

Anqi Tao received the B.S. degree in electrical engineering from Chongqing University, Chongqing, China, in 2020. She is currently pursuing the M.S. degree at the School of Electrical Engineering, Chongqing University. Her research interests include modeling, optimization, and allocation of distribution networks.

Niancheng Zhou received the B.S., M.S., and Ph.D. degrees in electrical engineering from Chongqing University, Chongqing, China, in 1991, 1994, and 1997, respectively. He worked at Chongqing Kuayue Technology Co., Ltd. in Chongqing from 1997 to 2003. He is a Professor at the School of Electrical Engineering, Chongqing University. From 2010 to 2011, he was a Research Fellow of Nanyang Technological University, Singapore. His research interests include analysis and operation of power systems, microgrids, and power quality.

Yuan Chi received the B.E. degree from Southeast University, Nanjing, China, in 2009, the M.E. degree from Chongqing University, Chongqing, China, in 2012, and the Ph.D. degree from Nanyang Technological University, Singapore, in 2021. From 2012 to 2016, he worked as an Electrical Engineer of Power System Planning consecutively with State Grid Chongqing Electric Power Research Institute, Chongqing, China, and Chongqing Economic and Technological Research Institute. He is currently working as a Research Associate with Chongqing University. His research interests include planning and resilience of power system and voltage stability.

Qianggang Wang received the B.S. and Ph.D. degrees from Chongqing University, Chongqing, China, in 2009 and 2015, respectively. He is currently an Associate Professor with the School of Electrical Engineering, Chongqing University. He was a Research Fellow with Nanyang Technological University, Singapore, from 2015 to 2016. His research interests include analysis and operation of power systems, microgrids, and power quality.

Guangde Dong received the B.S. and M.S. degrees from Chongqing University, Chongqing, China, in 2010 and 2013, respectively. He is currently a Senior Engineer with Electric Power Research Institute, State Grid Chongqing Electric Power Company Ltd., Chongqing, China. His research interests include energy saving, power quality analysis, and power system analysis.